A numerical study of the accuracy of single-electron current standards

L. R. C. Fonseca[a)]
Department of Applied Mathematics and Statistics, State University of New York at Stony Brook, Stony Brook, New York 11794-3600

A. N. Korotkov[b)] and K. K. Likharev
Department of Physics, State University of New York at Stony Brook, Stony Brook, New York 11794-3800

(Received 3 January 1996; accepted for publication 5 March 1996)

We have developed an algorithm for the analysis of single-electron standards of dc current. The algorithm is based on numerical solution of the master equation describing the time evolution of the probabilities of the electric charge states of the system, with iterative refinement of the operational set of states. To illustrate the method we have analyzed several standards of dc current. We have shown that the accuracy of the single-electron pump may be improved dramatically at lower frequencies and temperatures by replacing the traditional triangular drive wave forms with a special step-like drive. We have also shown that the M-junction turnstile does not achieve the accuracy of the 5-junction pump with the same values of capacitances and resistances even at $M=8$. However, a hybrid M-junction pump/turnstile system which is easier to control than the 5-junction pump, exhibits a comparable accuracy already at $M=6$. © *1996 American Institute of Physics.* [S0021-8979(96)01212-1]

I. INTRODUCTION

The ability to control single electrons in nanoscale circuits has opened the way to a new family of electronic devices.[1–4] These devices consist of one or several small conducting islands, separated from each other (and from external electrodes) by tunnel junctions. Because the capacitances of the islands are small, their electrostatic potentials are sensitive to the presence of extra single electrons/holes in the circuit. This sensitivity has suggested several applications of single-electron effects, including logic devices, memory cells, ultrasensitive electrometers, and dc current standards.[4]

While a crude description of single-electron devices within the framework of the semiclassical ''orthodox'' theory of correlated single-electron tunneling is quite simple,[1–3] the analysis of higher-order cotunneling processes[5] requires extensive computation. Earlier we developed an algorithm (dubbed ''SENECA,'' which stands for single-electron nanoelectronic circuit analyzer) for automated semi-quantitative analysis of these processes in arbitrary circuits.[6] It uses a Fokker–Plank type approach to handle transition rates which may differ from each other by many orders of magnitude. This is accomplished by solving a system of master equations[1] for the probability evolution of the various charge states of the system. The rates are calculated using the approximation suggested by Jensen and Martinis,[7] with several minor improvements.[6] The program searches for deviations from the predictions of the orthodox theory in an iterative way, such that only certain states are considered at each iteration. The choice of these ''operational'' states is based on their estimated mean probabilities. The original algorithm was applied to the study of leakage rates and dynamic errors in single-electron traps,[6] and can be used for studies of other devices without dc current.

In order to analyze devices with dc current, like the turnstile[8] or the pump,[9] the algorithm had to be extended, which was the main goal of this work. The new features include the determination of stationary probabilities of the charge states of the system, and a new procedure to cancel large terms of opposite sign without generating numerical noise. To demonstrate the capabilities of the extended code, we have carried out a preliminary study of the accuracy of the turnstile and the pump, which operate by passing one electron through the circuit per cycle of a periodic rf drive signal. Since metrological applications require an accuracy of the order of one part per billion,[7] these devices must be analyzed taking into account all sources of error, including those due to high frequency of the rf drive, thermal activation, and cotunneling.[5] As will be shown below, our algorithm presents a convenient means of tracking all these processes.

The paper is organized as follows. In Sec. II we discuss the new features introduced into SENECA. In Sec. III we analyze the 5-junction pump, while in Sec. IV we determine a nearly optimal set of parameters for the operation of the 8-junction turnstile and compare its accuracy with that of the pump. The last device, a hybrid pump/turnstile consisting of 6 tunnel junctions and 2 rf drives, is analyzed in Sec. V. Conclusions and a discussion of possible future studies are presented in Sec. VI. In the Appendix we describe the computer resources needed for the calculations discussed in the paper.

II. CHARGE STATES AND CURRENT CALCULATION

For the proper operation of single-electron circuits, the tunnel resistances R_t of all junctions should be high enough, $R_t \gg R_Q$, where $R_Q = h/e^2 \approx 25.8$ kΩ is the quantum unit of resistance. In this case the electron charge of each island is quantized, and a state of the circuit can be uniquely defined by its ''charge configuration,'' i.e., the set of numbers of

[a)]Present address: Beckman Institute for Advanced Science and Technology, University of Illinois, Urbana, IL 61801; Electronic mail: fonseca@ceg.uiuc.edu
[b)]Electronic mail: akorotkov@ccmail.sunysb.edu

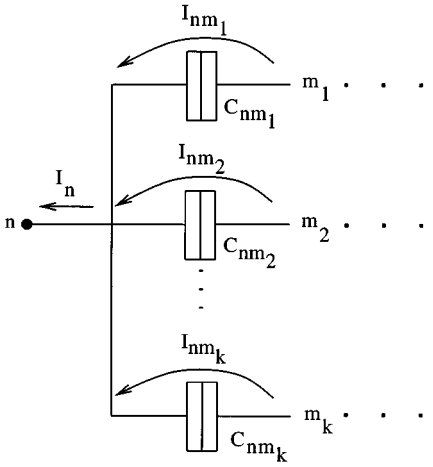

FIG. 1. The ''tunneling current'' through an external electrode is the current provided by tunneling events (arrows) in the junctions directly connected to the electrode.

(extra) electrons in the islands. When there is no dc current flowing through the device, it is natural to use the charge configuration in both internal islands and external electrodes. This is how the states were considered in the first version of the algorithm.[6] However, when dc currents are finite, this definition becomes inconvenient because the device may have many states which differ only by the number of electrons that have passed through it. All these states are physically similar and evolve in time in the same way. Thus, in the presence of dc currents, it is convenient to define a state by its internal charge configuration only. Any change in the external charges can be stored as additional information relevant only for the calculation of currents flowing through the device.

Let I_n be the current through external electrode n. It may be written as the sum of two parts, $I_n(t)=I_n^{tun}(t)+I_n^{ind}(t)$, where the first term is the current due to tunneling through the junctions connected directly to this electrode (Fig. 1), while the second term is the polarization-induced current due to tunneling through other junctions and the direct influence of rf drive wave forms. The first term is defined simply by[10]

$$I_n^{tun}(t)=e\sum_{i,j,\Delta k} P_i(t)\Gamma_{ij}^{\Delta k}(t)\Delta k_n, \tag{1}$$

where e is the electron charge, P_i is the probability of state i, and $\Gamma_{ij}^{\Delta k}$ is the rate of transition from state i to state j which leads to a transfer of charge $e\Delta k_n$ into external n.

The induced part of the current through external n can be calculated as

$$I_n^{ind}(t)=\frac{dQ_n^{ind}(t)}{dt}, \tag{2}$$

where the induced charge Q_n^{ind} is given by

$$Q_n^{ind}(t)=\sum_{i,m} P_i(t)C_{mn}V_{mn}(t). \tag{3}$$

The summation is over all states i, and all capacitances C_{mn} connected to external n (Fig. 1); V_{mn} are the voltages across capacitances C_{mn}.

Even though information on the instantaneous current can be helpful to understand the behavior of the device and sources of errors, the most important result is the average dc current. It can be obtained by just time-averaging equation 1 over one full cycle ($0\leqslant t\leqslant\tau$) of the external rf drive, since the average induced current is always zero. Thus,

$$I=\frac{e}{\tau}\int_0^\tau\sum_{i,j,\Delta k} P_i(t)\Gamma_{ij}^{\Delta k}(t)\Delta k dt, \tag{4}$$

where I is the vector of dc currents through the external electrodes and Δk is the vector of corresponding numbers Δk_n. For a discrete time approximation, $t_q=\Sigma_{p=1}^{q}\Delta t_p$, this expression may be rewritten as

$$I=\frac{e}{\tau}\sum_p \Delta t_p\sum_{i,j,\Delta k}\overline{P_i}(t_p)\Gamma_{ij}^{\Delta k}(t_p)\Delta k, \tag{5}$$

where the instantaneous probability $P_i(t)$ was substituted by the mean probability $\overline{P_i}(t_p)$ during each small time interval $[t_{p-1},t_p]$.

In practice, however, this method is useful only if I is far from a quantized level k_0ef, where $f=1/\tau$ is the rf drive frequency, and k_0 is an integer corresponding to the number of electrons that pass through the device per cycle in an ''ideal'' operation (without errors). The reason is that the current is calculated as a sum of several terms which may have considerable numerical noise due to finite accuracy in the calculation of P_i in equation 5, obscuring the real, smaller deviations from the quantized level. Rounding errors may also spoil the calculation of current deviation whenever I is closer to k_0ef than the machine double precision ($\sim 10^{-16}$ in our case).

In order to circumvent this problem, we have derived an expression for the current which explicitly separates the integer part of the current k_0ef from the current deviation

$$\Delta I=I-k_0ef. \tag{6}$$

Let us assign to each state i a vector of integers $k_i(t)$ with length equal to the number of external electrodes. The idea is to choose the k_i's in such a way that the cancellation of big currents in the expression for ΔI is exact since the subtraction occurs among integer numbers. For any choice of $k_i(t)$, equation 4 may be rewritten as follows:

$$\frac{I}{ef}=Q_1+Q_2, \tag{7}$$

where

$$Q_1=\int_0^\tau\sum_{i,j,\Delta k} P_i(t)\Gamma_{ij}^{\Delta k}(t)(\Delta k-k_j(t)+k_i(t))dt, \tag{8}$$

$$Q_2=\int_0^\tau\sum_{i,j} P_i(t)\Gamma_{ij}(t)(k_j(t)-k_i(t))dt, \tag{9}$$

and $\Gamma_{ij}(t)=\Sigma_{\Delta k}\Gamma_{ij}^{\Delta k}(t)$. Using the master equation of probability evolution[1,3,4,6] we can substitute

$$P_i \sum_j \Gamma_{ij} = \sum_j P_j \Gamma_{ji} - \dot{P}_i \tag{10}$$

into the part of equation 9 which is proportional to k_i. Integrating this term by parts, we obtain

$$Q_2 = -\sum_i \int_0^\tau P_i(t)\dot{k}_i(t)dt + [P_i(t)k_i(t)]|_0^\tau. \tag{11}$$

Using the facts that $P_i(\tau) = P_i(0)$ (periodic process) and that $\Sigma_i P_i = 1$, and discretizing time again, we obtain the final expression for the current:

$$\begin{aligned}\frac{I}{ef} = k_0 &+ \sum_p \Delta t_p \sum_{i,j,\Delta k} \overline{P_i}(t_p)\Gamma_{ij}^{\Delta k}(t_p)(\Delta k - k_j(t_p) \\ &+ k_i(t_p)) \\ &- \sum_p \sum_i \overline{P_i}(t_p)[k_i(t_p) - k_i(t_{p-1})] \\ &+ \sum_i P_i(0)[k_i(\tau) - k_i(0) - k_0].\end{aligned} \tag{12}$$

Equation 12 is formally valid for any choice of the numbers $k_i(t_p)$. However, if $k_i(t_p)$ are selected in such a way that the factors $(\Delta k - k_j(t_p) + k_i(t_p))$ are zero for processes that lead to the desired operation, then only small deviations from $k_0 ef$ will be left in equation 12 in addition to the quantized current $k_0 ef$ itself. In this case the fourth term in equation 12 is exactly zero since k_0 electrons per period pass through the device, hence $k_i(\tau) - k_i(0) = k_0$. In an error-free operation the third term is also zero since the change of $k_i(t_p)$ occurs only when $\overline{P_i}(t_p)$ is negligible.

The proper choice of vectors $k_i(t_p)$'s is generally not unique. In our algorithm they are defined in the following way: we take $k_1(0) = 0$ for the initial state (state 1) at $t = 0$. At the end of each time step when the rates and mean probabilities are known,[6] we set $k_j(t_p) = k_i(t_p - \Delta t_p) + \Delta k$, where Δk corresponds to the largest probability flux $P_i \Gamma_{ij}^{\Delta k}(t_p)$. At the quantized level of dc current, the set of largest probability fluxes corresponds to the path along the space of states which does not lead to error, and therefore the factors $(\Delta k - k_j(t_p) + k_i(t_p))$ corresponding to transitions which do not produce error cancel out.

This method was tested for many cases when the deviation of the current from the ideal value $ek_0 f$ was small. For example, Fig. 2 shows the device accuracy $|\Delta I/I|$ (here $k_0 = 1$) in the 5-junction pump using a step-like drive (see Sec. III) as a function of temperature. The dashed and solid curves were calculated using equations 5 and 12, respectively. We see that equation 12 is able to describe relative current deviations of the order of 10^{-19} (much smaller than the machine double precision) while equation 5 gives an error of the order of 10^{-11} (the minimum at $T \approx 6$ mK is evidently meaningless).

Another new feature of the algorithm is the determination of the stationary probabilities $P_j^{st}(t)$ of the charge states of the system, necessary for the calculation of current. The stationary probabilities were determined using a transfer matrix D, where D_{ij} is the conditional probability that the system arrives at state i at $t = \tau$ if the initial state at $t = 0$ is j. The vector of stationary probabilities P^{st} is the solution of the eigenvalue problem

$$DP^{st} = P^{st}. \tag{13}$$

Generally the determination of the matrix D and vector P^{st} has to be repeated for every iteration[6] after the first time a new state appears at $t = \tau$, since new rates calculated at each new iteration may change elements of the matrix D and thus the stationary probabilities. The direct calculation of the matrix D may be considerably time-consuming since it requires one passage through the time period for each initial state j. In the program we have the following shortcut option. At the end of each time step t_p the probability $P_i(t_p)$ of each state i obtained from the solution of the master equation 10 with initial condition $P_j(0) = 1$ is compared with the probability of the same state obtained in each of the previous passages with different initial states j. If these numbers differ, we continue normally to the next time step. If they are the same, it means that the system has returned to a state already visited in one of the previous passages, for which we know all the probabilities at $t = \tau$. CPU time is then saved by skipping the remaining time steps.

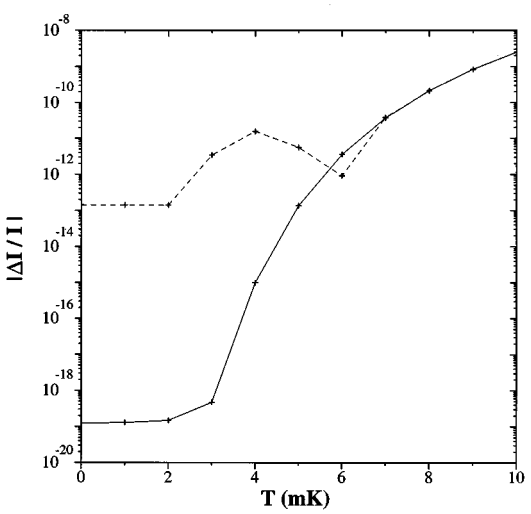

FIG. 2. dc current deviation from the quantized level ef in a 5-junction pump (Fig. 3) as a function of temperature calculated using equations 5 (dashed line) and 12 (solid line). The pump (with parameters $C = 0.1$ fF, $C_g/C \ll 1$, $R_t = 300$ kΩ, and $f = 1$ MHz) is driven by a step-like rf wave form (Sec. III). While the calculation using equation 5 gives errors of the order of 10^{-11}, the method using equation 12 is more accurate than the computer's double precision ($\sim 10^{-16}$). Here and below the accuracy of the results is limited by the approximation for the cotunneling rates (Ref. 6) and the lines connecting the data points are only guides for the eye.

III. PUMP

The first application of the algorithm discussed above was a preliminary optimization of the single-electron pump [Fig. 3(a)]. The dynamics of this M-junction system has been extensively studied[7–9,11,12] for the case where each rf drive input is sequentially fed by a triangular shaped wave form [see Fig. 3(b)]. The amplitude of each signal corresponds to induced charge $(Q_{g_i})_{min} = C_g(V_{g_i})_{min} = -e$ in each island

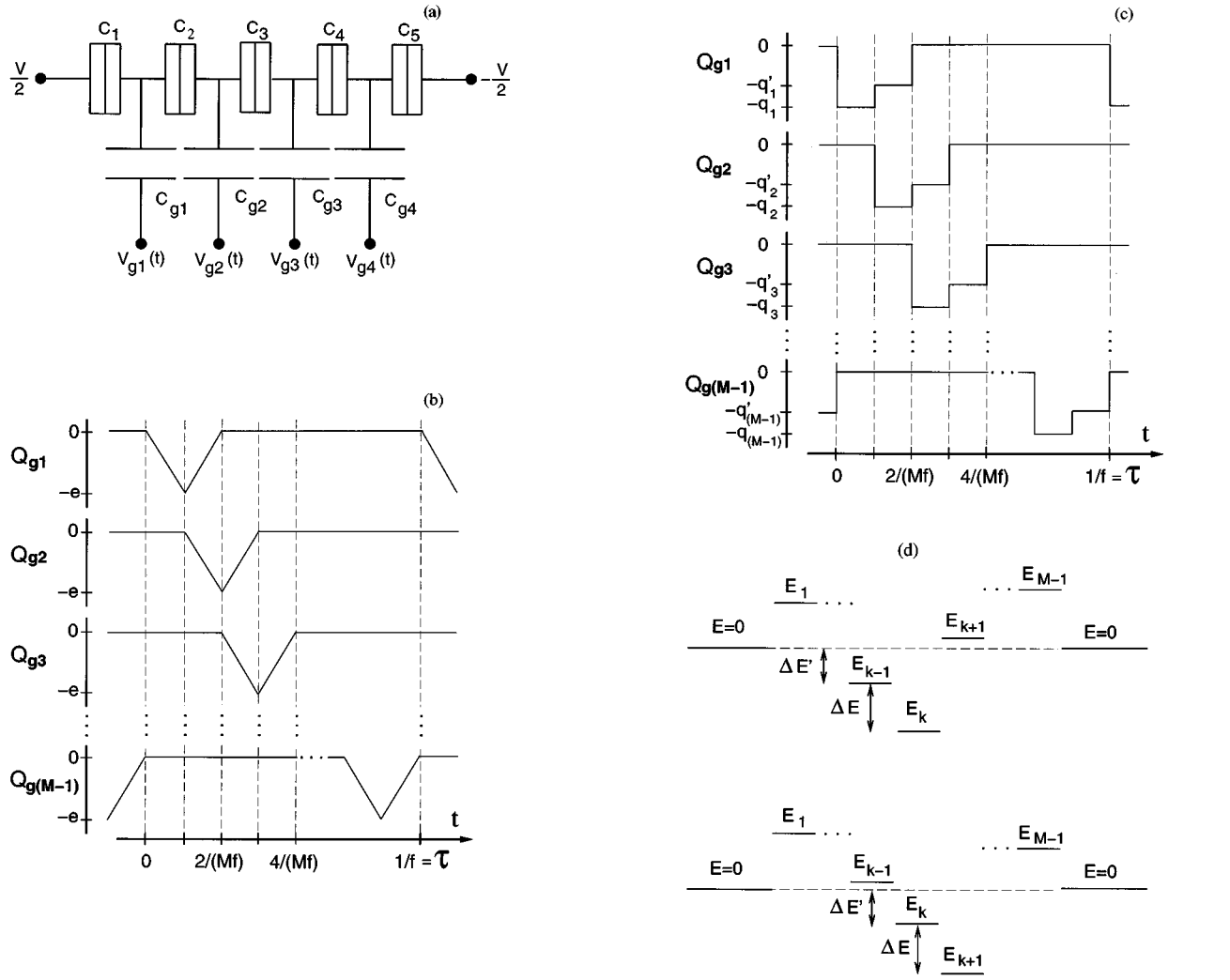

FIG. 3. (a) The 5-junction pump and possible wave forms of its rf drive: (b) usual triangular-shaped signal, (c) special step-like signal; (d) single-electron energy profile in the device driven by the step-like signal at two sequential steps of the rf drive.

i. The time shift between the triangular pulses applied to neighboring electrodes provides for the unidirectional transfer of one electron per period ($k_0=1$) between neighboring islands—see the inset in Fig. 4(a). For this mode, it has been estimated that a 5-junction pump with $C_i=0.1$ fF, $C_{g_i}\ll C_i$, and $R_t=300$ kΩ, could provide the accuracies $|\Delta I/I|\sim 10^{-14}$ at $T=10$ mK and $|\Delta I/I|\sim 10^{-11}$ at $T=100$ mK when operating at rf drive frequency of 10 MHz.[12] The reported accuracy of an experimental implementation of such a pump is at least two orders of magnitude worse than the theoretical prediction, apparently affected by technical factors like drift of background charge and noise from environment.[11] However, recent results[13] obtained for a similar system, the single-electron trap, suggest that these parasitic effects may be rather small. Our goal was to check the theoretical estimates for the triangular-shaped drive, and suggest methods of improving the ultimate accuracy of this device. We have not considered the effects of background charges in the analysis of the pump, as well as in any of the devices discussed later.

Figure 4 shows the total current $I(t)$ flowing through the right external electrode and the modulus of the relative current deviation $|\Delta I/I|$ from the classical process as functions of time for two different temperatures. The inset diagrams show the processes responsible for each peak. While the peaks in Fig. 4(a) result from classical tunneling between neighboring islands, those in Fig. 4(b) are created by fourth order cotunneling in the direction opposite to that of the classical current. Cotunneling events can only occur if the final state at each time step is not occupied, which means that they take place before the corresponding (and expected) classical tunneling events. Notice that in this particular case (zero dc voltage V), cotunneling creates a small current in the direction opposite to the classical current. Figure 4(b) also shows that each ''burst'' of cotunneling current contributes nearly the same amount to the total dc current deviation from the quantized level ef (if the gate capacitances C_g are comparable to C, this fact may not hold).

The fact that the total current through the unbiased pump is always slightly below ef suggests a simple way to im-

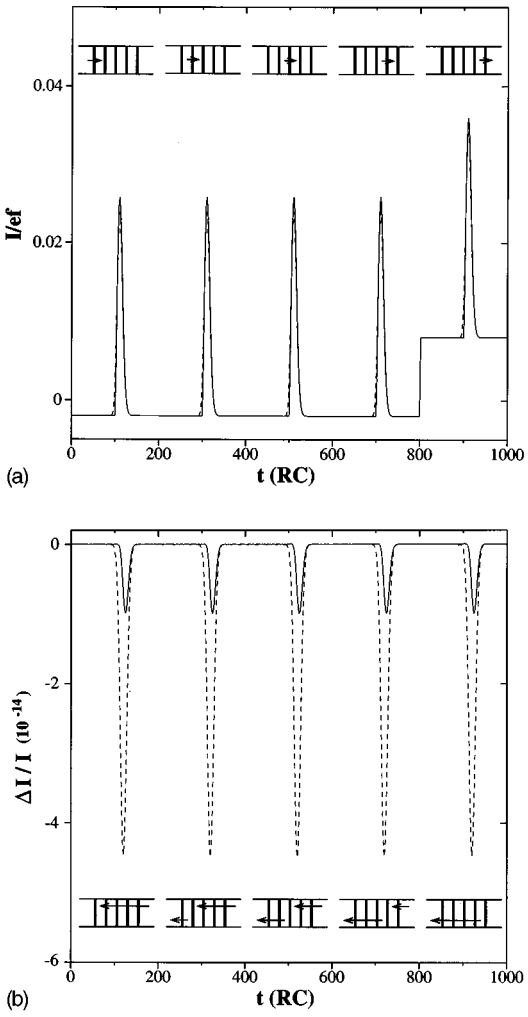

FIG. 4. (a) Total current through the right electrode in the 5-junction pump and (b) current deviation from the classical value due to cotunneling, as functions of time for a pump with small gate capacitances ($C_g/C \ll 1$) at $f=10$ MHz. Solid lines: $T=0$; dashed lines: $T=100$ mK. In (a) the flat plateaus of $I(t)$ are shifted from the origin due to the polarization-induced current given by equation 2. The shift is the same along the period of the rf drive since the rf signal has a triangular shape [Fig. 3(b)] and therefore the time derivative of $Q_n^{ind}(t)$ is a negative/positive constant in the first/second half of each pulse. The step in the induced current at $t=800RC$ is caused by the presence of only one triangular pulse after this instant [Fig. 3(b)]. Insets show the electron tunneling events responsible for each peak. $R_t=300$ kΩ, $C=0.1$fF. Here and below background charges in the islands are assumed to be compensated by additional dc voltages applied to the gates.

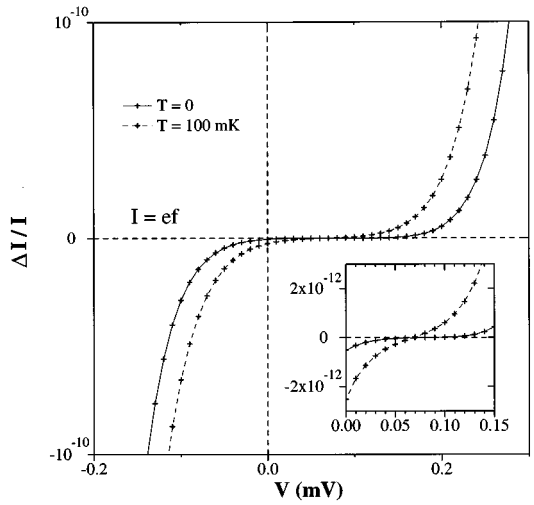

FIG. 5. Current deviation in the 5-junction pump driven by the triangular wave form ($f=10$ MHz) as a function of dc bias, showing the voltage offset of the plateau. The inset shows the same curves on an extended scale.

prove its accuracy, namely applying a small dc bias voltage V to the pump as a whole [Fig. 3(a)].[7] Figure 5 shows that the pump's dc current as a function of V exhibits a clear plateau at $I \approx ef$, shifted from the origin along the V axis. The existence of a plateau centered at $V>0$ means that the use of a finite bias does not introduce new errors that just cancel cotunneling errors at $V=0$, but actually drives the system closer to its ideal operation.

An important issue at this point is at which bias V the current deviation ΔI should be calculated. In our simulations we have chosen to calculate the deviation at the inflection point V_0 of the corresponding dc $I-V$ curve ($d^2I/dV^2|_{V=V_0}=0$) because this point does not depend on any arbitrary parameter and can be determined experimentally with reasonable accuracy. A difficulty with this choice arises when the bias point is located too close to the point where $I=k_0ef$ (the inflection point generally moves when parameters of the system are changed, and may cross the k_0ef level). Even though the current deviation is formally zero at such a crossing point, this fact cannot be used practically because the level k_0ef is not known *a priori*. In addition, in any experiment performed during a finite time interval $\tau'=M\tau$, there is a lower bound for the measurable current deviation imposed by fluctuations ($I_{rms} \sim \tau'^{-1/2}$) which have not been considered so far.

This problem can be circumvented artificially by smoothing the $|\Delta I/I|$ vs V curve in the region around the crossing point. A simple way to do that is to define the mean relative current deviation at the inflection point $\overline{\Delta I/I}$ as the average $|\Delta I/I|$ at three points, V_0 and $V_0(1\pm\kappa)$. Figure 6 shows an example of the application of this technique, where the crosses are $|\Delta I/I|$ as a function of bias voltage for the 5-junction pump. The circle shows $|\Delta I(V_0)/I|$, while the triangles pointing up and down mark the current deviations at $V=V_0(1\pm\kappa)$ for $\kappa=0.1$. The dotted line shows the mean $\overline{\Delta I/I}$ in this case. The choice of κ is rather arbitrary; however the mean value is reasonably insensitive to κ as long as it belongs to the interval $[0.05,0.20]$. For the sake of simplicity we will use the notation $|\Delta I/I|$ for the relative current deviation of both dc biased and unbiased devices; for the biased devices it will mean the average discussed above with $\kappa=0.1$. Our final Figs. 12 and 13 also show $|\Delta I/I|$ in all three points V_0 and $V_0(1\pm\kappa)$ (the notation is the same as in Fig. 6).

Figure 12 shows, among other results, the comparison of the accuracy of the unbiased (solid line) and dc-biased (dotted line) 5-junction pump as a function of temperature for $f=10$ MHz. The inflection point V_0 varies from ~ 80 μV at $T=0$ to ~ 50 μV at $T=200$ mK. We see that the dc bias may provide a considerable accuracy improvement (a factor

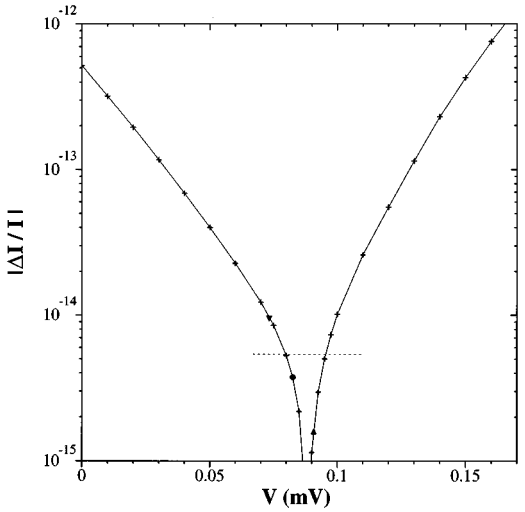

FIG. 6. Current deviation in the 5-junction pump at low temperatures and $f=10$ MHz. Crosses: calculated values of $|\Delta I(V)/I|$; circle: the inflection point V_0; triangle up (down): $V=V_0(1\pm\kappa)$, with $\kappa=0.1$; dotted line: average of the last three points.

of ~ 100 for temperatures below 50 mK and of ~ 10 for temperatures between 100 mK and 200 mK). The improvement decreases as temperature increases, since thermal activation over the energy barrier created by the array as a whole eventually becomes the main source of error (independent of bias voltage) instead of cotunneling. Note that the calculated accuracy of the unbiased pump at 10 mK is about two orders of magnitude worse than in earlier estimates,[12] while at 100 mK it agrees well with those predictions. Because the ''error bars'' connecting the four points are in most cases longer towards smaller values of the current deviation, it is possible to conclude that the mean $\overline{\Delta I}/I$ is a rather conservative estimate of the device error.

Figure 13 shows the comparison of the current deviation in unbiased (solid line) and biased (dotted line) 5-junction pumps as a function of frequency at low temperatures. We see that the dc bias provides a two-order-of-magnitude improvement along the full range of frequencies analyzed.

The use of a non-triangular rf drive wave form, e.g. a step-like signal, may offer a second way to improve the operation of the pump. While tunneling only starts some time after the beginning of a triangular pulse and the classical tunneling rate grows linearly with time after that, a step-like signal allows classical tunneling to start at the beginning of the step with the maximum classical rate.

The particular step-like signal used in our calculations is shown in Fig. 3(c). The induced charges q_k and q'_{k-1} in neighboring islands were chosen in the following way: the energy difference between the state with one electron in island k and all other islands empty, and the state with one electron in island $k-1$ and all other islands empty, is ΔE (independent of k). The energy difference between the state with one electron in island $k-1$ and the state without any electron in the circuit is $\Delta E'$, is also independent of k [Fig. 3(d)]. (The exceptions are the charges induced in the edge islands: q_1 for which $\Delta E'=0$, and q_M for which $\Delta E'=-\Delta E$.)

In order to avoid cotunneling in the direction opposite to the classical current, ΔE should be reduced until the dynamic error becomes comparable to the cotunneling error. The well-known expression[1] for the rate of classical tunneling $\Gamma=\Delta E/(R_t e^2)$ shows that in order to have the probability of dynamic error less than some value ϵ, the energy difference ΔE between final and initial states has to satisfy the following inequality:

$$\Delta E > m e^2 f R_t \ln\frac{1}{\epsilon}, \tag{14}$$

where $m=\tau/\Delta t$ is the number of time steps per period τ. The cotunneling rate can be calculated analytically in some very simplified cases. For example, let us consider the case of an array of M identical tunnel junctions (with identical capacitances $C_i=C$ and resistances $R_{ti}=R_t$), small gate capacitances, and zero temperature. Let the external bias applied to the system be larger than but very close to the threshold $e(M-N)/2C$ $(N\leqslant M)$, such that the lowest order of cotunneling transition which decreases the energy of the system is N. Because V is close to the threshold, the energy difference between initial and final states is small. Thus the energies of the electron–hole pairs in each island created by cotunneling are negligible,[5] which allows the Nth order cotunneling rate to be estimated as

$$\Gamma^{(N)}=\frac{2\pi}{\hbar}\alpha^N\left(\frac{2MC}{e^2}\right)^{(2N-2)}\left(\frac{N}{(N-1)!}\right)^2\frac{\Delta E^{2N-1}}{(2N-1)!}, \tag{15}$$

where $\alpha=\hbar/(2\pi e^2 R_t)$. The upper bound for ΔE can now be easily obtained, requiring that the probability of cotunneling be also less than ϵ

$$\Delta E < g(\alpha,N,M)(mf\epsilon)^{\frac{1}{2N-1}}, \tag{16}$$

where

$$g(\alpha,N,M)=\left\{\frac{\hbar}{2\pi}\alpha^{-N}\left(\frac{e^2}{2MC}\right)^{(2N-2)}\left(\frac{(N-1)!}{N}\right)^2 \times(2N-1)!\right\}^{\frac{1}{2N-1}} \tag{17}$$

does not depend on f or ϵ. (In order to operate at non-zero temperatures, the energy difference ΔE should be increased to avoid thermally-induced errors. A comprehensive analysis of this case, as well as the optimization of the junction's resistances R_t for given T and f are in progress and their results will be the subject of a separate publication). The dashed lines in Fig. 7(a) show the bounds given by equations 14 and 16 for the 5-junction pump at 1 MHz and 10 MHz (the lowest order of cotunneling possible is $N=M-1=4$). The crossing point of these bounds sets the nearly-optimal value of ΔE for each frequency.

Fixing ΔE to the value of the crossing point (10, 80, and 500 μeV at $f=1$, 10, and 100 MHz, respectively), we now vary $\Delta E'$. By changing $\Delta E'$ we are essentially changing the height of two energy barriers for electron transfer:

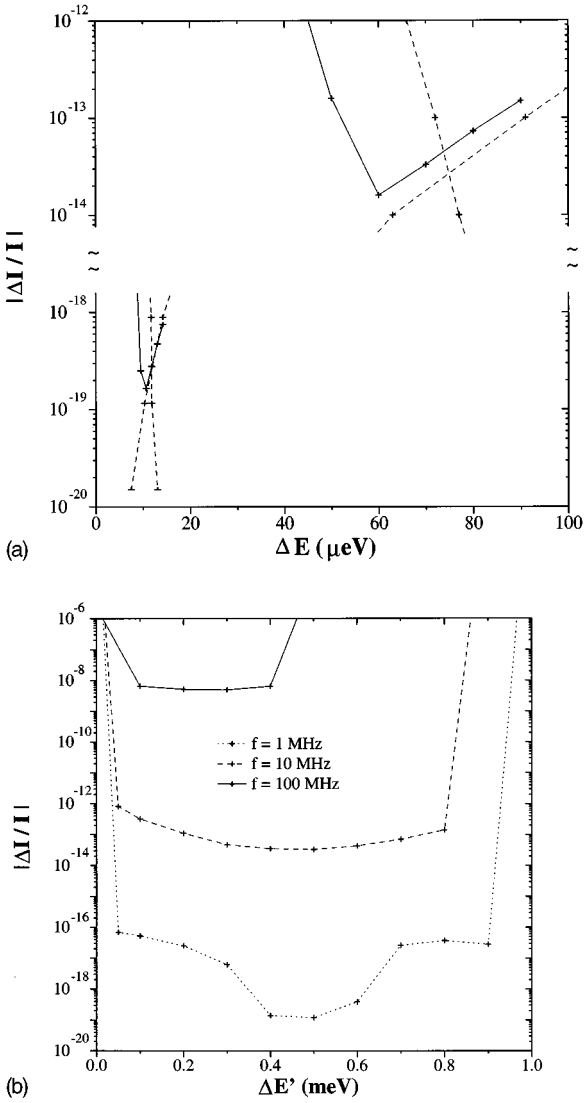

FIG. 7. (a) Current deviation in the 5-junction pump as a function of ΔE [Fig. 3(d)] at 10 MHz (upper right) and 1 MHz (lower left) at fixed $\Delta E' = 0.5$ meV. Solid lines: numerical calculations; dashed lines: analytical estimates. (b) Current deviation as a function of $\Delta E'$ at fixed ΔE (10, 80, and 500 μeV at 1, 10, and 100 MHz, respectively). In (a) and (b), $T = 0$.

small $|\Delta E'|$ implies a lower barrier for processes with an intermediate state of zero electrons in the pump, while for large $|\Delta E'|$ processes with an intermediate state of two electrons in the pump are favorable. Figure 7(b) shows the current deviation as a function of $\Delta E'$ for these three frequencies. Because the accuracy depends only weakly on $\Delta E'$, we can now fix it at 0.5 meV for $f = 1$ and at 10 MHz, and 0.3 meV for $f = 100$ MHz, and make a final tuning of ΔE around the value used before. The solid curve in Fig. 7(a) shows the result of this final iteration. The agreement between the numerical results and the analytical calculations is reasonably good, both for the optimal ΔE and the best accuracy attainable at a given frequency. Note that at optimal values of ΔE and $\Delta E'$, the amplitude of the effective charge $Q_{ef} = C_g(U_i + U_{i+1})$ injected into both islands turns out to be close to $-e$, just like in the triangular wave form case.

The comparison between the accuracy of the dc-

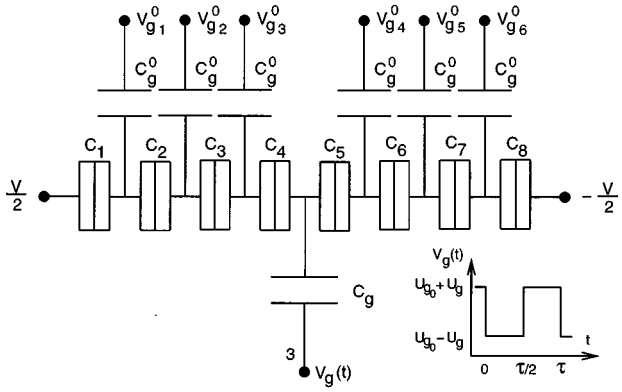

FIG. 8. The 8-junction turnstile. For $C = 0.1$ fF, the ''good'' gate capacitance is $C_g = 18$ aF.

unbiased pump driven by the triangular (solid line) and step-like (long-dash line) wave forms as a function of frequency for low temperatures is presented in Fig. 13. The logarithm of the current deviation grows almost linearly with the logarithm of the frequency in both cases, but the slope of the curve for the step-like wave form is larger (approximately proportional to f^6, compared to f^3 for the triangular wave form), yielding a better accuracy at low frequencies. Indeed, using the step-like wave form the accuracy of the pump at $f = 10$ MHz and 1 MHz ($\sim 10^{-14}$ and $\sim 10^{-19}$, respectively) may be about 20 and 10^4 times better than the accuracy using the triangular pulses.

IV. TURNSTILE

The M-junction turnstile[8] (Fig. 8) is another candidate device for a standard of dc current. It consists of an array of M tunnel junctions with one rf drive source connected to the central island via a capacitance C_g. The other islands are connected to external electrodes i by small gate capacitances C_g^0 ($C_g^0/C \ll 1$) to compensate background charges with dc voltages V_{gi}^0 [in rf driven islands, such compensation can be achieved by dc offsets of $V_{gi}(t)$]. In contrast to the pump, a dc bias voltage $V \neq 0$ is necessary for the proper operation of the turnstile. Indeed, V determines the direction of electron transfer in the first half of the cycle, when the rf potential applied to the central island lowers its electron addition energy. (The entrance of more electrons is blocked by the Coulomb repulsion created by the first electron, as long as the amplitude of the rf signal is not too large.) In the second half of the time period, the potential in the middle island is increased until the electron escapes into the right electrode.

The turnstile is an attractive choice for a standard of dc current due to the smaller number of parameters to optimize, which makes it simpler than the pump. It has been argued based on theoretical estimates[12] that a 10-junction turnstile with no stray capacitances could be operated with the maximum accuracy of $\sim 10^{-12}$. The goal of our work was to check these estimates. So far we have only analyzed turnstiles containing 6 and 8 similar junctions and no stray capacitances. (Devices containing more than 5–7 junctions

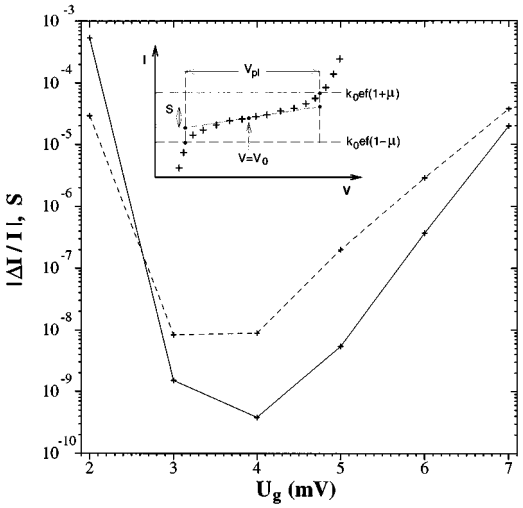

FIG. 9. Optimization of the rf gate amplitude U_g in the 8-junction turnstile for the fixed gate capacitance $C_g=4C/3N$ and dc gate amplitude $U_g^0=e/2C_g$ at $T=0$ and $f=1$ MHz. The solid and dashed lines show the current deviation at the inflection point and the plateau slant S, respectively. The inset illustrates the definition of the plateau slant.

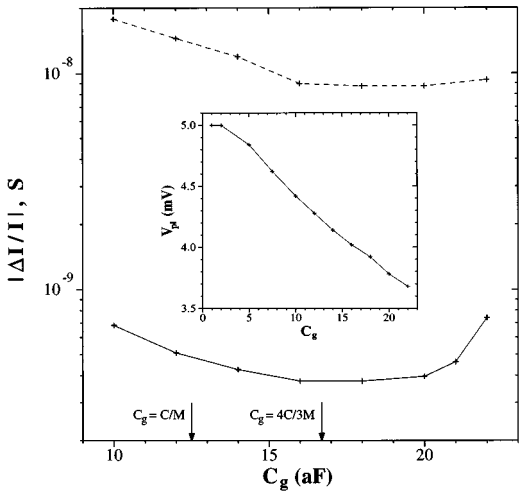

FIG. 10. Current deviation (solid line), plateau slant (dashed line), and plateau length (inset) in the 8-junction turnstile as functions of the gate capacitance at $T=0$ and $f=1$ MHz. Induced charge is kept fixed ($Q_g=C_gU_g=0.42e$), and dc gate amplitude $U_g^0=e/2C_g$ is changed accordingly.

may suffer seriously from the limitations imposed by stray capacitances[13] which were not considered in the previous estimates either.)

In our simulations we used a step-like rf drive wave form (inset in Fig. 8), which delivers a better performance for the turnstile than the triangular wave form.[14] In order to perform a partial optimization of the turnstile's parameters we first determined the best rf gate amplitude U_g for some fixed choice of gate capacitance C_g (which also fixes the optimum dc gate voltage,[12] $U_g^0=e/2C_g$), low temperature and frequency. Using the resulting U_g, we varied C_g while keeping the induced charge in the central island $Q_g=C_gU_g$ fixed. These nearly-optimal values of U_g and C_g were then kept fixed as temperature and frequency were varied.

Good operating devices are characterized by long and flat $I-V$ curve plateaus. Therefore, in the following discussion, along with the relative current deviation $\Delta I/I$, we will use the concept of the ''slant'' of the plateau, defined as (see the inset in Fig. 9)

$$S=\frac{dI(V_0)}{dV}\,\frac{V_{pl}}{k_0ef}, \tag{18}$$

where $dI(V_0)/dV$ is the slope at the inflection point and V_{pl} is the plateau length. V_{pl} is obtained from a classical calculation at $T=0$, where we define that points in the $I-V$ curve belong to the plateau if they differ from k_0ef by less than μk_0ef, where μ is a small parameter. In our calculations we used $\mu=10^{-2}$, but the results are rather insensitive to variation of this parameter.

Figure 9 shows the dependence of the current deviation at the inflection point (solid line) and S (dashed line) on the rf amplitude U_g (in these calculations we again assumed $C=0.1$ fF and $R_t=300$ kΩ) at $T=0$ and $f=1$ MHz. The gate capacitance is $C_g=16.6$ aF, calculated from the relation $C_g=4C/3M$, which is supposed to be nearly optimal.[12] The minima of S and $|\Delta I/I|$ occur approximately at the same value of U_g, corresponding to the inserted charge $Q_g=C_gU_g\approx 0.5e$. Notice that this value is twice smaller than in the pump. We assumed $U_g=4.0$ mV ($Q_g=0.42e$) as a ''good'' amplitude.

The inset in Fig. 10 shows the classical calculation of the plateau length V_{pl} as a function of C_g at a fixed dc induced charge $Q_g=0.42e$ with the dc gate bias $U_g^0=e/2C_g$ being changed accordingly. It shows that the smaller the gate capacitance the longer the plateau. The reason is that the charging energy decreases with the total island capacitance which includes the gate capacitance. However, a calculation of the current deviation and plateau slant (Fig. 10) shows that when cotunneling is taken into account the use of a very small C_g is not the best choice. The current deviation has a minimum at $C_g\approx 18$ aF, very close to the theoretical estimate $C_g=4C/3M$ by Averin *et al.*,[12] which can be explained as follows. The total capacitance of the middle island decreases as C_g decreases; the result is an increase in the energy difference between the state of zero electrons in the device and the state of one electron in the middle island (in the first and second half of the cycle), promoting cotunneling processes that lead to error. At the same time, the energy difference between the state of zero electrons in the device and the state of one electron in the first island (in the first half of the cycle), and between the state of one electron in the middle island and the state of one electron in the next island to the right (in the second half of the cycle) also increases, decreasing dynamic error. Therefore, the minimum observed in Fig. 10 results from an optimal value of C_g for which the rates of dynamical and cotunneling errors are the same. The dependence of the current deviation on the gate capacitance is rather weak, though, and it seems that any choice of C_g close to C/M (Fig. 10) is almost equally satisfactory.

Figures 12 and 13 show, among other results, how the relative current deviation in the quasi-optimized turnstile varies with temperature and frequency, respectively (dot–dashed lines in both figures). The loss of accuracy at high

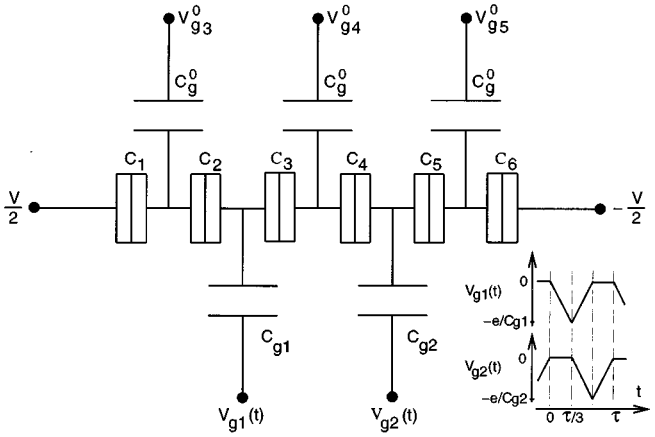

FIG. 11. The 6-junction *h*-pump and wave forms of its two rf drives.

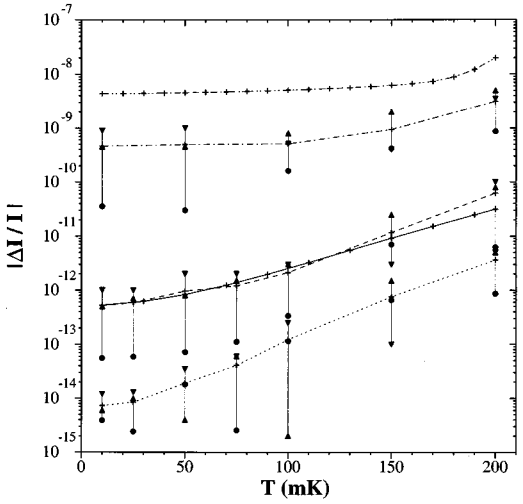

FIG. 12. Current deviations in the unbiased (solid line) and biased (dotted line) 5-junction pump (both driven with a triangular wave form), unbiased (dot–dot–dashed line) and biased (dashed line) 6-junction *h*-pump driven with the same triangular wave form, and the 8-junction turnstile driven by a step-like wave form (dot-dash line) at $f=10$ MHz as functions of temperature. Circles: current deviation at inflection point V_0; triangles up (down): current deviation at $V_0(1\pm0.1)$; crosses denote the current deviation at $V=0$ in unbiased devices and the average current deviation in biased devices (for discussion, see Sec. III).

temperature is due to thermally activated jumps over the energy barrier created by island charging, while at high frequency it is caused by the increasing dynamic error (probability that the electron misses a rf cycle). At small T and f, cotunneling is the main source of error.

V. THE HYBRID PUMP/TURNSTILE

The system of external voltages that drives electrons through single-electron devices should be optimized considering all its variables simultaneously, since each gate potential generally changes all island charges due to crosstalk.[11] Thus the experimental time of search for the optimal point in the corresponding parameter space grows exponentially with the number of parameters. The system of voltages controlling the M-junction pump has $3\times(M-1)$ parameters to optimize, namely one dc bias (to compensate the background charge), one rf amplitude, and one rf phase at each of the $(M-1)$ external electrodes, yielding 12 parameters for $M=5$. The M-junction turnstile with only one time-dependent wave form depends on $(M-1)$ dc biases, one rf amplitude, one rf phase, and one bias voltage applied to the circuit as a whole (Fig. 8), summing up to $(M+2)$ parameters. For $M=8$ (the case described in Sec. IV) there are 10 parameters. This is less than in the 5-junction pump, but the accuracy of this device is lower too.

In order to decrease the number of parameters to optimize and still have an accuracy comparable to that of the M-junction pump, let us consider a hybrid pump/turnstile device, which we call the *h*-pump (Fig. 11). The idea is to add more tunnel junctions to the array and reduce the number of rf drives.

The *h*-pump operates by first decreasing the potential V_{g1} (Fig. 11) in the first external electrode until one electron tunnels from the left electrode to the second island and is trapped there. The potential V_{g1} is then increased at the same time V_{g2} is decreased, resulting in the tunneling of the electron from the second island to the fourth island. Finally, V_{g2} is increased until the electron is ejected from the fourth island to the right electrode. Both rf biased electrodes are connected to the circuit by small gate capacitances C_g $(C_g/C\ll1)$. The remaining external electrodes $i=1,2,\ldots,$ are connected to the device by small gate capacitances C_g^0 $(C_g^0/C\ll1)$ to compensate background charges with dc voltages V_{gi}^0. As in the pump, various rf drive wave forms can be used to drive electrons across the h-pump. In this study we have only used the triangular wave form, with rf amplitude $(U_g)_{min}=(Q_g/C_g)_{min}=-e$, as in the usual pump (we have checked that this value is close to optimal).

We have considered the *h*-pump with 6 tunnel junctions and 2 rf drives. In this case the number of parameters is reduced to 10 (five dc amplitudes, two rf drive amplitudes, two rf drive phases, and one dc bias voltage). In Fig. 12 we compare the relative current deviations in the *h*-pump operating with zero dc bias (dot–dot–dashed line) and finite dc bias in the inflection point (dashed line) as functions of temperature at 10 MHz with the accuracies of other devices. Notice that while the unbiased *h*-pump performs poorly, the dc-biased one provides an accuracy comparable to that of the unbiased 5-junction pump.

Figure 13 shows the comparison of the current deviation in the *h*-pump operating at finite bias (dashed line) as a function of frequency (at low temperature) with other dc current standards. Notice that the accuracy of the biased *h*-pump is better than the accuracy of the unbiased 5-junction pump at frequencies higher than 10 MHz.

VI. CONCLUSION

We have described an algorithm suitable for the calculation of very small dc current deviations from the quantized levels $I=k_0ef$ in several single-electron devices, for various rf drive frequencies f and temperatures T. To show its capabilities we have carried out a preliminary study of the possible accuracy of several standards of dc current, including a

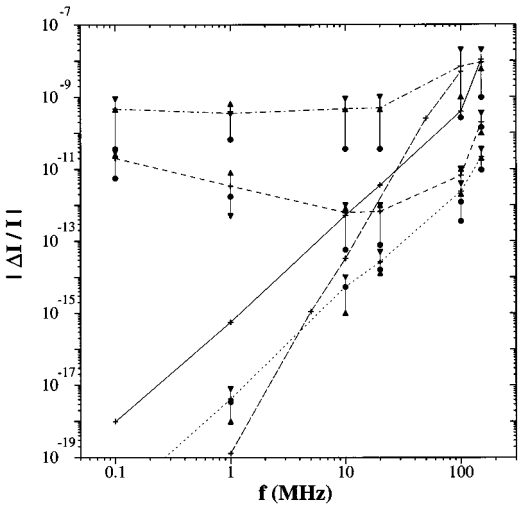

FIG. 13. Current deviations in unbiased 5-junction pump with triangular (solid line) and step-like (long-dash line) rf drive wave forms, biased 5-junction pump with triangular wave form (dotted line), biased 6-junction *h*-pump with triangular wave form (dashed line), and 8-junction turnstile with step-like wave form (dot–dashed line) at $T=0$ as functions of drive frequency. The notation is the same as in Fig. 12.

5-junction pump, an 8-junction turnstile, and a hybrid 6-junction pump/turnstile device (''*h*-pump''). We selected the parameters $C=0.\ 1$ fF and $R_t=300\ \text{k}\Omega$ for all devices.

For the 8-junction single-electron turnstile using a relatively good set of parameters and a step-like rf wave form, we obtained a final accuracy of only $\sim 10^{-9}$, with a weak dependence on f and T. This (relatively) poor accuracy results from the fact that, in order to pass one electron through the circuit per cycle of the rf drive, a large dc voltage applied to the array as a whole and/or a large rf amplitude applied to the middle island are necessary, favoring undesirable cotunneling transitions.

The accuracy of the 5-junction single-electron pump driven by a triangular rf wave form is much better: at $f=10$ MHz the relative error $\Delta I/I$ is $\sim 10^{-12}$ for low temperatures and $\sim 10^{-11}$ for $T=200$ mK. At low temperatures, its accuracy ranges between $\sim 10^{-18}$ and $\sim 10^{-8}$ for frequencies between 100 kHz to 150 MHz, growing with frequency as f^3 (this dependence follows from the analytical estimates made in Sec. III).

The analysis of the pump has suggested two ways of improving its accuracy. In the first, a small bias was applied to the device in order to balance the backward cotunneling current. This technique applied to a 5-junction pump may provide an improvement of $\Delta I/I$ of two orders of magnitude in a wide range of frequencies (0.1–150 MHz) at low temperatures. For $f=10$ MHz, the improvement is about one order of magnitude for temperatures between 100 and 200 mK, and of two orders of magnitude for temperatures below 50 mK.

In the second technique, the traditional triangular pulses were substituted by a step-like wave form crafted to balance dynamic errors and cotunneling errors. This balance results in a stronger frequency dependence of the device error, $\Delta I/I \propto f^6$. Using this wave form optimized only for low temperatures, the accuracy of the pump at $f=10$ MHz and 1 MHz ($\sim 10^{-14}$ and $\sim 10^{-19}$, respectively) is about 20 and 10^4 times better than the accuracy obtained using the triangular pulses.

Finally we have shown that the operation of a new device, the ''*h*-pump,'' with 6 junctions and dc bias may be approximately as accurate as the operation of the unbiased 5-junction pump for temperatures between 0 and 200 mK ($f=10$ MHz) and even better for frequencies higher than 10 MHz at low temperatures. At the same time, the *h*-pump has a smaller set of parameters to optimize in experimental practice.

To summarize, our results show that the limitations on the accuracy of typical single-electron devices imposed by dynamic errors, cotunneling and thermal activation may be kept well below one part per billion. Notice, however, that we have performed only a crude search for optimal parameters of these devices in the multidimensional parameter space, rather than their thorough optimization. For example, we have not optimized the shape of the rf wave form. Moreover, the tunneling resistances R_t of all devices were kept fixed at 300 kΩ, regardless of temperature, frequency, and numbers of tunnel junctions. Small R_t increases cotunneling errors while large R_t increases dynamic errors. Thus the optimum value of R_t should be lower for higher frequencies and larger number of tunnel junctions. Our plans are to carry out such optimization of dc current standards in the near future.

ACKNOWLEDGMENTS

Numerous fruitful discussions with D. Averin, R. Chen, K. Matsuoka, and A. Odintsov are gratefully acknowledged. One of the authors (L.F.) would like to thank A. Grossi and A. McCoy for their valuable input on parallel algorithms. The work was supported in part by AFOSR and ONR/ARPA.

APPENDIX: COMPUTER REQUIREMENTS

Computer time and memory required by SENECA for most of the analyses discussed in this paper are within the reach of modern workstations. For example, the calculation of the current deviation in the unbiased 5-junction pump operating at 10 MHz and 100 mK, and driven by the triangular wave form discretized in 100 time steps, took ~15 seconds on a SGI INDIGO 2 workstation and required ~2 MB of memory.

The analysis of dc biased devices, especially those with more than 6–7 junctions, is a more time demanding operation. The reason is that in order to calculate the mean current deviation $\overline{\Delta I}/I$, the inflection point V_0 has to be determined, which requires calculating $\Delta I/I$ at several values of V around V_0 (~10 points are necessary). For example, to analyze the 6-junction *h*-pump, using the same parameters as before, the CPU time to calculate $\Delta I/I$ was about 90 minutes and the required memory was ~7 MB. Because 10 points were used to determine the inflection point, the scaled time was ~9 minutes per point, which is a factor of 40 larger than the time spent to calculate current deviation in the unbiased 5-junction pump.

Of course the addition of only one junction to the system cannot fully explain this difference. The main reason is that in the *h*-pump (as well as in the turnstile) the control over the charge states along the array is weaker than in the usual pump since there are only two gate electrodes (only one in the turnstile). This fact results in cascades of intermediate short-lived charge states which connect high probability states, inflating the size of the matrix of tunneling rates and hence the CPU time used for the solution of the master equation.[6] In the case of the 8-junction turnstile, CPU times as high as 2 hours per dc voltage point (thus $\sim$20 hours per $\overline{\Delta I}/I$ point) were needed for its analysis, even though the number of time steps was only 2 for the step-like rf drive wave form used.

To overcome these problems, SENECA has been extended to work on more advanced platforms, namely networks of heterogeneous workstations running under PVM,[15] and massively parallel processors (MPPs). The problems that can be solved by combinations of heterogeneous platforms should not involve intensive communication among processors, since local area networks are usually slow and workstations generally present different work loads and speed. A problem solvable by this approach is the calculation of the current deviation in a large number of independent points to generate a curve, each point taking an acceptable time. For simulations that require a lot of time per point, as described above, the use of a MPP seems more adequate. To do that, we have parallelized the solution of the master equation using the scalable universal matrix multiplication algorithm (SUMMA).[16] Using this method, we could reduce the CPU time per each point $\overline{\Delta I}/I$ from $\sim$20 hours to $\sim$2 hours using 16 nodes of the Intel Paragon.

We could not achieve a better speedup because the rest of the code is not easily parallelizable and still takes a considerable amount of computer time. Since most of the program only runs on a single processor, a master–slave model was used in which tasks are spawned to other nodes when necessary. This model limits the size of the problems that can be solved in a MPP to the available memory in one node, unless one uses the other nodes to store data, which does not seem to be a natural choice in our case. Thus, for the Intel Paragon we have used, the limiting memory is $\sim$26 MB. Using a fast workstation with more memory available as the master and the nodes of a MPP as the slaves, all running under PVM for example, could reduce the memory limitation dramatically, and therefore larger circuits could be analyzed in a reasonable time scale. This approach has not yet been tried.

[1] D. V. Averin and K. K. Likharev, in *Mesoscopic Phenomena in Solids*, edited by B. Altshuler (Elsevier, Amsterdam, 1991), p. 173.
[2] K. K. Likharev, IBM J. Res. Dev. **32**, 144 (1988).
[3] *Single Charge Tunneling*, edited by H. Grabert and M. H. Devoret (Plenum, New York, 1992).
[4] D. V. Averin and K. K. Likharev, in Ref. 3, p. 311.
[5] D. V. Averin and A. A. Odintsov, Phys. Lett. A **140**, 251 (1989).
[6] L. R. C. Fonseca, A. N. Korotkov, K. K. Likharev, and A. A. Odintsov, J. Appl. Phys. **78**, 3238 (1995).
[7] H. D. Jensen and J. M. Martinis, Phys. Rev. B **46**, 13 407 (1992).
[8] L. J. Geerligs, V. F. Anderegg, P. A. M. Holweg, J. E. Mooij, H. Pothier, D. Esteve, C. Urbina, and M. H. Devoret, Phys. Rev. Lett. **64**, 2691 (1990).
[9] H. Pothier, P. Lafarge, C. Urbina, and M. H. Devoret, Europhys. Lett. **17**, 249 (1992).
[10] I. O. Kulik and R. I. Shekhter, Zh. Éksp. Teor. Fiz. **68**, 623 (1975) [Sov. Phys. JETP **41**, 308 (1975)].
[11] J. M. Martinis, M. Nahum, and H. D. Jensen, Phys. Rev. Lett. **72**, 905 (1994).
[12] D. V. Averin, A. A. Odintsov, and S. V. Vyshenskii, J. Appl. Phys. **73**, 1297 (1993).
[13] P. D. Dresselhaus, L. Ji, J. E. Lukens, and K. K. Likharev, Phys. Rev. Lett. **72**, 3226 (1994).
[14] S. M. Verbrugh, Ph.D. thesis, Delft University of Technology, 1995.
[15] A. Geist, A. Beguelin, J. Dongarra, W. Jiang, R. Manchek, and V. Sunderam, *PVM: Parallel Virtual Machine. A Users' Guide and Tutorial for Networked Parallel Computing* (The MIT Press, Cambridge, 1994).
[16] R. A. van de Geijn and J. Watts (unpublished).